NEOPLASIA
www.neoplasia.com
Volume 14 Number 9 September 2012 pp. 788–798 788

High-resolution Whole-Genome Analysis of Skull Base Chordomas Implicates FHIT Loss in Chordoma Pathogenesis[1,2]

Roberto Jose Diaz[*,†,‡,3], Mustafa Guduk[§,3], Rocco Romagnuolo[*], Christian A. Smith[*], Paul Northcott[*], David Shih[*], Fitim Berisha[¶], Adrienne Flanagan[#,¶], David G. Munoz[**], Michael D. Cusimano[‡,††], M. Necmettin Pamir[§] and James T. Rutka[*,†,‡]

*Arthur and Sonia Labatt Brain Tumor Research Centre, The Hospital for Sick Children, Toronto, Ontario, Canada; [†]Department of Laboratory Medicine and Pathobiology, University of Toronto, Toronto, Ontario, Canada; [‡]Division of Neurosurgery, Department of Surgery, University of Toronto, Toronto, Ontario, Canada; [§]Department of Neurosurgery, Acibadem University, Istanbul, Turkey; [¶]Histopathology Department, Royal National Orthopaedic Hospital, Stanmore, Middlesex, UK; [#]UCL Cancer Institute, London, UK; **Keenan Research Centre, Department of Pathology, St. Michael's Hospital, Toronto, Ontario, Canada; [††]Division of Neurosurgery, Department of Surgery, St. Michael's Hospital, Toronto, Ontario, Canada

Abstract

Chordoma is a rare tumor arising in the sacrum, clivus, or vertebrae. It is often not completely resectable and shows a high incidence of recurrence and progression with shortened patient survival and impaired quality of life. Chemotherapeutic options are limited to investigational therapies at present. Therefore, adjuvant therapy for control of tumor recurrence and progression is of great interest, especially in skull base lesions where complete tumor resection is often not possible because of the proximity of cranial nerves. To understand the extent of genetic instability and associated chromosomal and gene losses or gains in skull base chordoma, we undertook whole-genome single-nucleotide polymorphism microarray analysis of flash frozen surgical chordoma specimens, 21 from the clivus and 1 from C1 to C2 vertebrae. We confirm the presence of a deletion at 9p involving *CDKN2A*, *CDKN2B*, and *MTAP* but at a much lower rate (22%) than previously reported for sacral chordoma. At a similar frequency (21%), we found aneuploidy of chromosome 3. Tissue microarray immunohistochemistry demonstrated absent or reduced fragile histidine triad (FHIT) protein expression in 98% of sacral chordomas and 67% of skull base chordomas. Our data suggest that chromosome 3 aneuploidy and epigenetic regulation of *FHIT* contribute to loss of the FHIT tumor suppressor in chordoma. The finding that FHIT is lost in a majority of chordomas provides new insight into chordoma pathogenesis and points to a potential new therapeutic target for this challenging neoplasm.

Neoplasia (2012) 14, 788–798

Abbreviations: FHIT, fragile histidine triad; SNP, single-nucleotide polymorphism

Address all correspondence to: James T. Rutka, MD, PhD, FRCSC, Suite 1503, Division of Neurosurgery, Department of Surgery, The Hospital for Sick Children, 555 University Avenue, Toronto, Ontario M5G 1X8, Canada. E-mail: james.rutka@sickkids.ca

[1]This work was supported by the Canadian Institutes of Health Research. Dr Diaz is a Canada Vanier Graduate Scholar at the University of Toronto.
[2]This article refers to supplementary materials, which are designated by Tables W1 and W2 and Figure W1 and are available online at www.neoplasia.com
[3]These two authors contributed equally to this work.
Received 16 March 2012; Revised 9 August 2012; Accepted 13 August 2012

DOI 10.1593/neo.12526

Introduction

As a primary tumor of the notochord-derived axial skeleton, chordoma is a rare entity with incidence ranging from 0.051 to 0.8 per 100,000 persons per year [1–3]. Because of the predilection for sacral and skull base lesions, surgical resection is often incomplete. The remnant tumor cells, although slowly growing, eventually reform the tumor bulk and can progress to a more malignant state with metastatic deposits to bone, lung, or liver [3–7]. Chemotherapeutic or biologic therapies for the treatment of chordoma are in preclinical and early clinical trials, with no curative therapy presently available to patients [8]. Proton beam radiation to the surgical bed has been shown beneficial with increased progression-free survival [9,10]; however, our understanding of the radiobiology and chemotherapeutic resilience of chordoma is incomplete.

Unbiased surveys of the chordoma genome can serve as a strategy for the generation of novel hypotheses about tumor pathogenesis and therapy as well as adding to our understanding of genetic aberrations unique to chordoma or common to other cancers. As such, this type of study serves to develop a basic knowledge of the fundamental alterations in the DNA code, which are associated not only with chordoma but also with neoplasia in general. In the setting of chordoma, it also serves to interrogate the genetic landscape in cells that are believed to originate from primitive notochord remnants. Multiple techniques for genetic analysis have been applied to chordoma previously including G banding, comparative genomic hybridization (CGH), fluorescence *in situ* hybridization (FISH), and spectral karyotype analysis. These studies have identified normal karyotypes in a majority of chordomas [11], a greater propensity for chromosomal losses [12], and documented the absence of consistent structural chromosomal aberrations in all chordomas. Aberrations in chromosomes 1, 3, 4, 12, 13, and 14 have been associated with chordoma recurrence [11,13,14]. Chromosomal changes have also been documented in chromosomes 2, 5, 6, 7, 9, 10, 17, and 20 [15–18]. The biologic significance of 1q and 9p loss and 7q gain and implications for therapeutic intervention have been recently reviewed [8]. Aberration of chromosome 3 by G banding analysis has been observed in 62% of skull base chordomas and complete loss of chromosome 3 or the 3p arm has been reported in chordoma with a frequency of 50% to 75% by CGH [12,19,20]. However, no specific tumor suppressor gene on chromosome 3 has yet been associated with chordoma.

In this study, whole-genome single-nucleotide polymorphism (SNP) microarray analysis was used to survey the genomic landscape of skull base chordomas. We document aneuploidy of chromosome 3 in tumors from 3 of 18 patients with a diagnosis of primary classic clival chordoma and in one recurrent tumor. The tumor suppressor fragile histidine triad (*FHIT*) resides on chromosome 3p14.2 and has been implicated in cancers in tissues arising from all three germ cell layers. Screening for changes in FHIT protein expression in skull base and sacral chordomas on tissue microarrays showed a significant level of reduced FHIT expression that may have important implications for chordoma pathogenesis and therapy.

Materials and Methods

Patients and Tumor Tissues

Patients diagnosed with skull base lesions with imaging features suggestive of chordoma or their surrogate decision maker in the case of pediatric patients gave informed consent for investigational use of tumor tissue. Patient samples were derived from the neurosurgical service in the Institute of Neurologic Sciences, University of Marmara (Istanbul, Turkey; n = 22) and at St. Michael's Hospital (Toronto, Ontario, Canada; n = 4). Ethical approval for investigational use of tumor tissue was obtained from the Committee for Ethical Medical Research of the University of Marmara and the St. Michael's Hospital Research Ethics Board. Tumor specimens obtained at the time of surgical resection were frozen in liquid nitrogen or fixed in formaldehyde. A pathological diagnosis was made by immunohistology and hematoxylin and eosin (H&E) histology by the neuropathologist. Chondroid chordomas were differentiated from classic chordomas by the presence of a hyaline cartilaginous matrix [21,22].

DNA Extraction and Quality Control

Genomic DNA from 22 fresh frozen tumors was isolated by sodium dodecyl sulfate/Proteinase K tissue digestion followed by phenol extraction and stored in tris-ethylenediaminetetraacetic acid (TE) buffer as described previously [23]. The quality of the DNA samples was evaluated by agarose gel electrophoresis before submission to The Centre for Applied Genomics, The Hospital for Sick Children (Toronto, Ontario, Canada) for hybridization to the Affymetrix Human Mapping 500K platform.

SNP Array and Data Analysis

DNA from 22 samples was prepared as previously described [23] and hybridized to Affymetrix Human Mapping 500K Arrays (Affymetrix, Santa Clara, CA), which are comprised of an Sty array and an Nsp array. The Sty array is capable of genotyping approximately 238,000 SNPs, whereas the Nsp array can genotype approximately 262,000 SNPs. Data analysis was performed using dChip 2006 [24,25] and CNAG 2.0 [26] software applications. CEL files were imported into dChip, and the probe signals were quantile normalized and modeled. Raw copy number estimates were generated using normal diploid samples from Marshall et al. [27] and subsequently segmented using the circular binary segmentation (CBS) algorithm [28]. The segmented copy number profiles were visualized in IGV [29]. Focal deletions and amplifications were defined as gain or loss of >10 SNPs and <12 Mb in size. The list of gene loci showing focal deletion or amplification was then analyzed using Ingenuity Pathways Analysis (Ingenuity Systems, www.ingenuity.com) for gene function, identification of canonical pathways, and gene network determination.

Tissue Microarray and Tissue Section Immunohistochemistry

A skull base chordoma and a sacral chordoma tissue microarray was immunostained for FHIT protein using rabbit anti-FHIT (HPA018840; Sigma, St Louis, MO) antibody at 1:30 dilution on a Leica BOND-MAX machine using the Leica Polymer Refine Kit (Leica Microsystems, Wetzlar, Germany). Pretreatment was done for 20 minutes using Leica ER2 solution. The positive control was normal kidney tissue. Immunostaining for the FHIT protein on the tissue microarray was scored by Dr Flanagan. A second pathologist (Dr Roberto Tirabosco) scored the samples blinded to the results of the first scoring. Staining data were available on 85 sacral and 49 skull base tumors. The staining intensity recorded was converted into a graded scale with the following values (0—none, 0.5—equivocal, 1—minimal, 2—moderate, 3—intense). The average score from two core samples if available was determined. The frequency of samples falling into each category of staining was determined, and Chi-square analysis was performed to determine statistical significance at a P value of .05 in frequency within each category between sacral and skull base chordomas. To assess for tissue heterogeneity in FHIT expression, we performed immunohistochemistry on sections from a set of four chordomas for which tumor-positive blocks were

available. Formalin-fixed paraffin-embedded sections were obtained at a thickness of 4 μm. Sections were dewaxed in paraffin and rehydrated through decreasing concentration of ethanol. Antigen retrieval was performed by heating in citrate buffer (pH 6.0). Endogenous peroxidase activity was blocked with hydrogen peroxide. Rabbit anti-FHIT (HPA018840; Sigma) was used at a dilution of 1:30. Vector Elite avidin-biotin complex method detection system (Vector Laboratories, Burlington, Canada) was used with 3,3′-diaminobenzidine as the chromogenic substrate and hematoxylin as counterstain. Slides were visualized and photographed using a Leica DM4500B microscope and reviewed by a neuropathologist (Dr Munoz).

Results

The present study includes genomic analysis of 22 tumor samples including one recurrent tumor (12 females and 9 males; median, 38 years; range, 12 to 83 years; Table 1). Nineteen of the tumors were diagnosed as classic chordoma, whereas three were chondroid chordoma. Twenty-two tumors were located in clivus and one was located at the C1 to C2 vertebral level. Twenty-one tumors were primary lesions, whereas one was a local recurrence of tumor 6 years after initial resection (CHD20, primary is CHD19). Additionally, three primary chordomas and one recurrent clival chordoma (two males and two females; range, 22–78 years) were assessed for FHIT expression by immunohistochemistry of whole tissue sections. Core samples from sacral and skull base chordomas were assessed for FHIT protein expression by immunohistochemistry on tissue microarrays as described in Materials and Methods. These samples originated from patients in the United Kingdom over long time periods and no clinical data were available for analysis.

Table 1. Patient Demographics and Tumor Features.

ID	Age	Sex	Location	Pathology
CHD1	32	M	Clivus	Classic
CHD2	42	F	Clivus	Classic
CHD3	65	M	Clivus	Classic
CHD6	12	F	Clivus	Classic
CHD7	13	F	Clivus	Classic
CHD8	22	F	Clivus	Classic
CHD9	36	M	C1–C2	Chondroid
CHD10	26	F	Clivus	Classic
CHD11	83	F	Clivus	Classic
CHD12	63	F	Clivus	Classic
CHD13	55	F	Clivus	Chondroid
CHD14	22	F	Clivus	Chondroid
CHD15	51	M	Clivus	Classic
CHD16	42	F	Clivus	Classic
CHD17	35	M	Clivus	Classic
CHD18	38	M	Clivus	Classic
CHD19	31	F	Clivus	Classic
CHD20	37	F	Clivus	Classic, Recurrence of CHD19
CHD21	43	M	Clivus	Classic
CHD22	35	F	Clivus	Classic
CHD23	65	M	Clivus	Classic
CHD26	50	M	Clivus	Classic

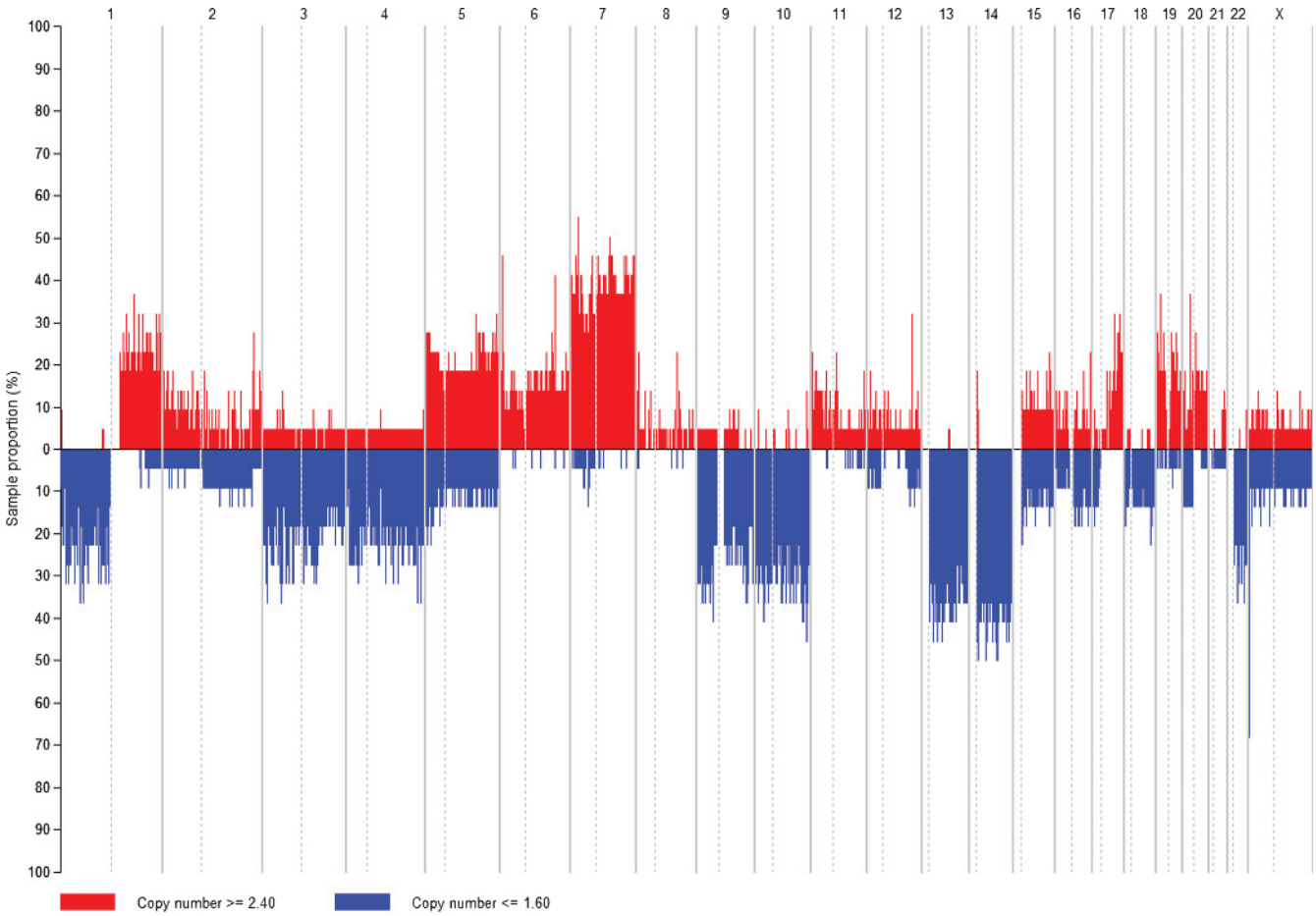

Figure 1. Frequency of DNA copy number changes detected by SNP array analysis in 22 skull base chordomas. Losses were more frequent than gains.

Whole-genome SNP analysis shows that losses are more frequent than gains in skull base chordomas. At a deletion *z*-score > 2 or <0.5 and *q*-value < 0.05, the following deletions were identified as having broad significance: 3p (661 genes), 3q (732 genes), 9p (275 genes), 9q (731 genes), 10p (248 genes), 10q (817 genes), 13q (400 genes), 14q (874 genes), and 22q (598 genes). The significant chromosomal gains identified were 7p (390 genes), 7q (815 genes), 19p (721 genes), and 19q (1055 genes). Amplification and deletion frequencies, *z*-scores, and *q*-scores are provided in Table W1. The frequency of DNA copy number changes detected by SNP analysis with their genomic positions is shown in Figure 1, and genomic imbalances detected for individual tumor samples are shown in Figure 2. Focal amplifications (n = 43) were more commonly observed than focal deletions (n = 25) as listed in Table W2. Only three focal deletions (9p: 21.800–22.032 Mb, 3 genes; 15q: 18.427–20.060 Mb, 15 genes; 23: 0.019–2.700 Mb, 0 gene) and one focal amplification (14: 19.273–19.490 Mb, 6 genes) were observed in 2 or more of the 22 chordomas analyzed. Chromothripsis was observed in 2 of 18 primary clival chordomas (CHD8 and CHD1) on chromosomes 7 and 22, respectively (Figure 3). A total of 370 genes were found in focal amplifications and 98 genes in focal deletions. Ingenuity pathway analysis could be performed on 305 of 370 (82%) focally amplified genes and 96 of 98 (98%) of the focally deleted genes.

The three most common functions for genes found within focally amplified regions were cell morphology, apoptosis, and cell-cell signaling and interaction. A total of 14 amplified gene networks (>10 genes) were identified with five overlapping networks having major nodes of interaction with *TGFB1*, *NFKBIA*, *STAT1*, *SMAD 3*, and *CTNNB1*. Analysis of canonical pathways affected by gene amplification revealed alterations in embryonic stem cell developmental signaling and DNA methylation pathways (Figure 4, *A* and *B*). Importantly, we observed a focal amplification (6q: 164.424–170.748 Mb) involving the T-gene locus in 1 of 18 (CHD17) primary classic clival chordomas and amplification of a large segment of chromosome 6 containing the T-gene (6: 0.110391–170.748 Mb) in 4 of 18 primary classic clival chordomas and 1 of 3 primary chondroid skull base chordomas. Focally deleted genes mapped onto four gene networks (>10 genes) with the most frequent function within these networks being cell cycle regulation. Furthermore, the canonical pathways most frequently affected by focal gene deletion were those involved in cell cycle checkpoint control (Figure 4*C*). Importantly, we observed focal deletion of *CDKN2A*, *CDKN2B*, and *CHEK2* genes.

A 199,276,135-bp loss of chromosome 3 that includes the *FHIT* gene (chr3: 59,735,035–61,237,132) was observed in 3 of 19 classic chordoma (CHD17, 20, 26) specimens. This same region was amplified in 1 of 19 classic chordomas (CHD3). Acquired loss of

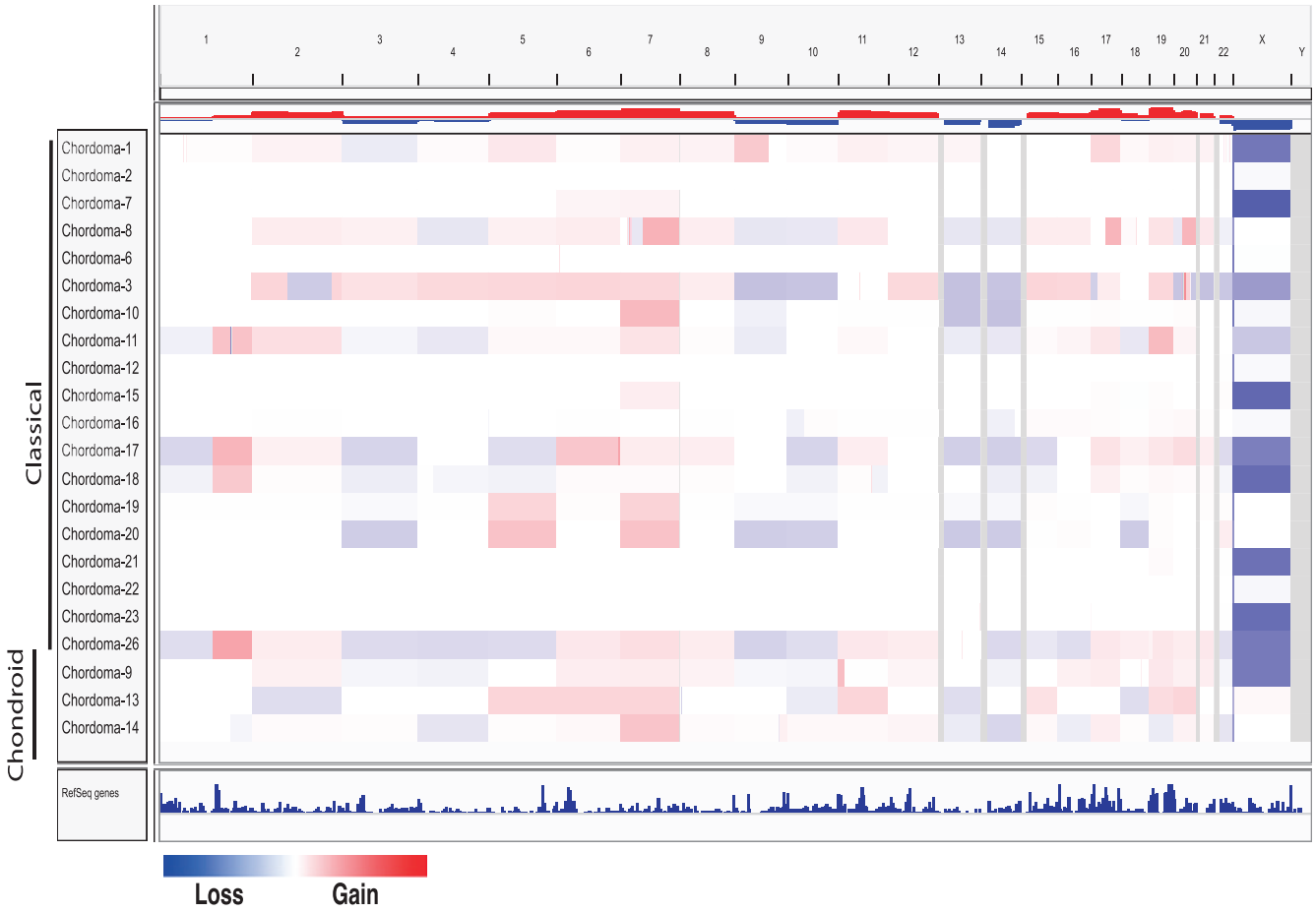

Figure 2. Genomic imbalances detected in individual tumor samples. Gains (red) and losses (blue) of genomic material were detected in all tumor samples by SNP array analysis. Each row corresponds to a unique sample and each column represents a specific chromosome. Chondroid and classic chordoma samples have been grouped to facilitate comparison. Note the acquisition of chromosome 3 loss and the similarity of gains and losses in the recurrent tumor sample (CHD20) to the primary tumor sample (CHD19).

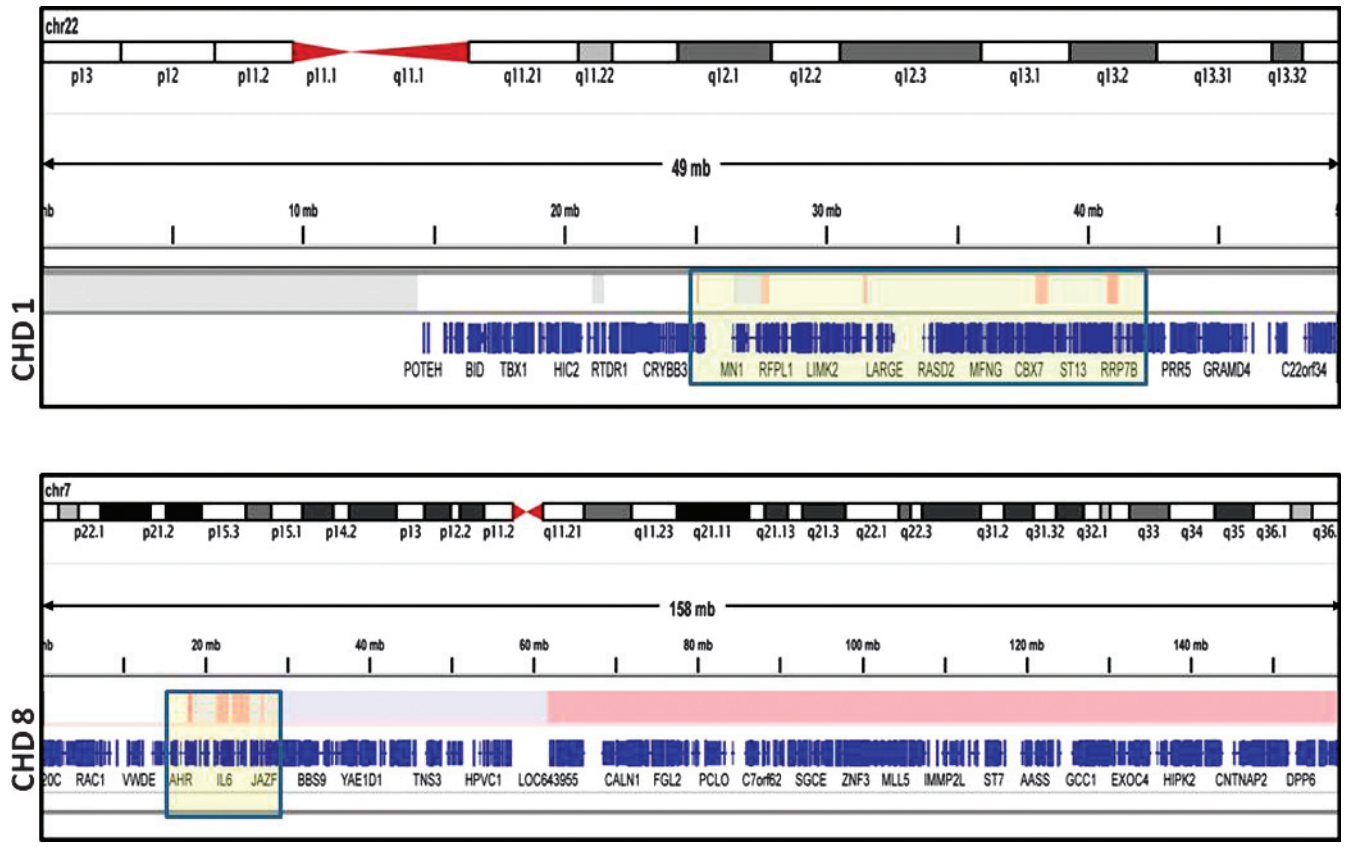

Figure 3. Map of chromothripsis found in chromosome 22 in CHD1 and chromosome 7 in CHD8. There are 43 genes affected on chromosome 22 and 32 genes affected on chromosome 7.

chromosome 3 is observed in a classic chordoma at recurrence (CHD20) 76 months after first resection but was not observed at the time of initial surgery (CHD19). Minimal, equivocal, or no FHIT immunostaining was observed in 83 of 85 (98%) sacral chordomas and 33 of 49 (67%) skull base chordomas. In addition, the FHIT expression profile is significantly different in sacral chordomas compared to skull base chordomas ($P < .001$), demonstrating a broad range of FHIT protein expression in skull base chordomas (Figure 5). The staining pattern of FHIT in clival chordoma is cytoplasmic and nuclear with prominence of nucleolar staining. Variation in staining intensity was observed between tumors (Figure 6, *B–E*) and within tumors (Figure 6, *E* and *F*). In regions of inflammation within the tumors, macrophages that had very intense nuclear and cytoplasmic staining that was much more prominent than staining in adjacent physaliferous chordoma cells were observed (Figure 6*F*).

Discussion

There are few genome-wide studies of chordomas. In a recent review of the literature, only 82 chordomas are reported with karyotype analysis [30]. Most chordomas have been reported to have near-diploid or moderately hypodiploid karyotypes [12]. Aneuploidy in chordoma has been a feature associated with poor clinical outcome for many years [31,32]. Recently, skull base chordomas with abnormal karyotypes were demonstrated to have higher recurrence rates (45% *vs* 3%) at an average of 48 months follow-up and were associated with shorter patient survival [11]. The largest series of whole-genome analysis has 30 classic chordoma tumor samples obtained from the sacrum, coccyx, or thoracic vertebra of 26 patients [12]. In that study, 15 of the cases had deletions affecting chromosome 9p21.3 covering the CDKN2A locus, which were identified by array CGH, FISH, or G banding. In our study, we also found 9p deletions involving regions that included the CDKN2A locus in 4 of 18 (22%) primary classic clival chordomas (Figure W1). More specifically, CHD3 showed a homozygous (235,401 bp) focal deletion and CHD8 a heterozygous focal deletion (426,901 bp), encompassing *C9orf53*, *CDKN2A*, and *CDKN2B* genes completely and the *MTAP* gene incompletely. Thus, whereas CDKN2A loss is observed in a small proportion of clival chordomas, it is much less frequent than that reported for sacral chordomas (70%) [12]. Scheil et al. have studied 16 chordomas (10 sacrococcygeal, 5 sphenooccipital, 1 spinal) by CGH and verified DNA sequence losses most prevalently at 3p (five of seven primary tumors) and 1p, whereas gains were observed on chromosomes 20, 7q, 5q, and 12q [19]. Sawyer et al. found cytogenetic abnormalities in 11 of 22 skull base and cervical chordoma samples by using G banding and spectral karyotyping methods. Karyotype abnormalities occurred exclusively in recurrent tumors and the recurrent alterations involved isochromosome 1q and monosomy of chromosomes 3, 4, 10, 13, and 18 [14]. In our study, we found isochromosome 1q (4 of 18), chromosome 3 loss (3 of 18), and 7q gain (11 of 18) in primary skull base chordoma samples that support the validity of the data set. Comparison of broad significance copy number changes observed in this study with those previously reported shows that chromosome 7 gains and chromosome 3 losses are observed in both sacral and clival chordomas, whereas sacral chordomas have several unique chromosomal losses and gains, which are not observed in our series of clival chordomas (Table 2) [12,19,33]. Another important observation is that there appears to be greater genomic copy

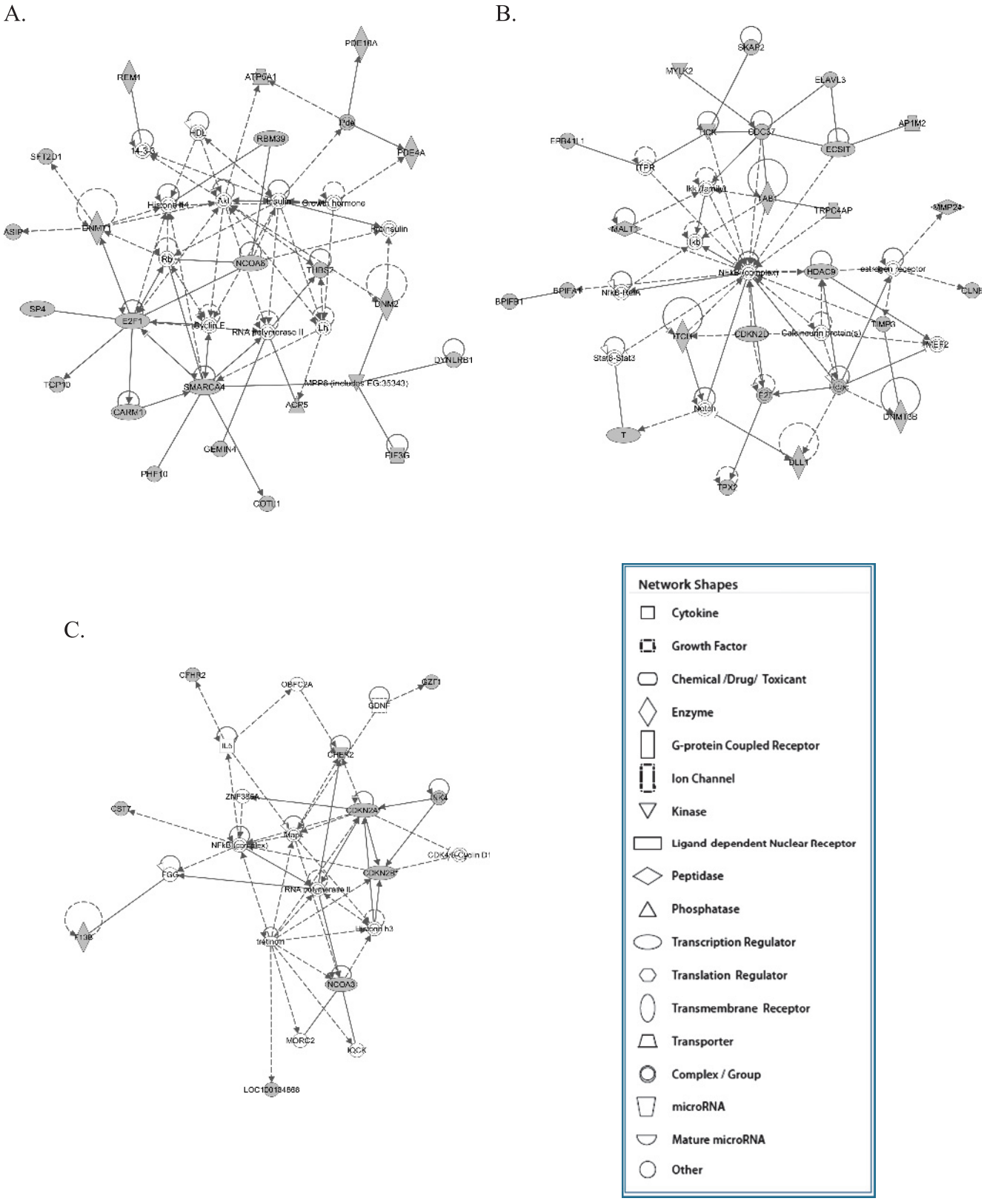

Figure 4. Gene network maps for the top networks formed by genes found (A, B) within focal amplifications and (C) within focal deletions. Gray nodes indicate deleted or amplified genes, whereas white nodes are interacting genes not part of focal amplifications or deletions. Solid lines indicate direct protein interaction. Solid arrows indicate direct action on and dashed arrows indicate indirect action on.

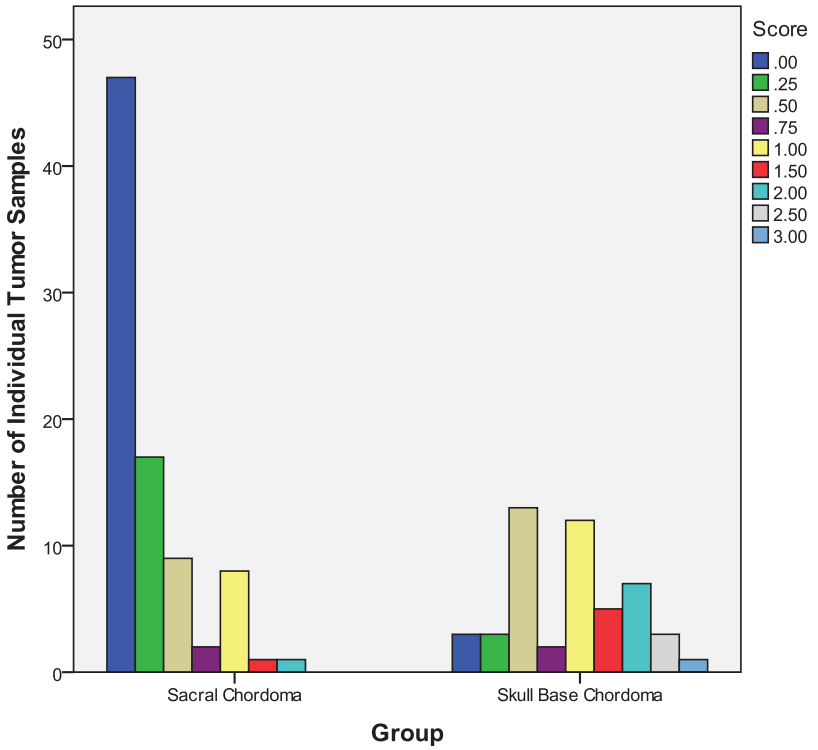

Count

		SCORE									Total
		.00	.25	.50	.75	1.00	1.50	2.00	2.50	3.00	
Group	Sacral chordoma	47	17	9	2	8	1	1	0	0	85
	Skull base chordoma	3	3	13	2	12	5	7	3	1	49
Total		50	20	22	4	20	6	8	3	1	134

Figure 5. Histogram showing tissue microarray scoring for FHIT protein immunostaining in skull base and sacral chordomas. A score of 0 represents no staining, 0.5 equivocal staining, 1 minimal staining, 2 moderate staining, and 3 intense staining.

number alterations in sacral chordomas, which are seen in an older patient population, compared to the clival chordomas that are found in a younger patient population (Table 2). Although there were no frequent recurrent copy number alterations in the clival chordomas analyzed, we identified focal amplifications and deletions encompassing gene networks that mapped to specific functional domains. Ingenuity pathway analysis demonstrated that gene loci located within amplifications were associated with embryonic stem cell signaling and DNA methylation, whereas genes located within focal deletions were primarily involved in cell cycle regulation. The importance of embryonic stem cell signaling in chordoma has been highlighted recently by the finding that gain of the T-gene locus is not only present in familial but also sporadic chordoma and that T-gene expression is required for chordoma cell proliferation *in vitro* and *in vivo* [34–36]. Furthermore, the observation of stem cell behavior in chordoma cells expressing the CD133 stem cell marker further supports the importance of stem cell signaling in chordoma [37]. The T-gene amplification frequency ranges from 0% to 54% in studies with mixed populations of sacral, spinal, and clival sporadic chordomas. In this study, 5 of 18 (28%) primary clival chordomas showed copy number gain of the T-gene. This suggests that while clival chordomas share pathogenetic mechanisms similar to those previously reported in genomic studies biased toward sacral chordomas, Brachyury expression in some of these tumors may be a result of epigenetic changes triggered by initiating genomic events other than T-gene amplification.

Deletion, rearrangement, or loss of heterozygosity in 3p is frequently reported in lung [38–41], renal [42], nasopharyngeal [43], cervical [44], and breast cancers [45]. We have observed a chromosome 3 gain or loss encompassing an ~200-Mb region mapping to 3p26.3-3q26.1 in 4 of 19 (21%) classic skull base chordomas. This observation is in keeping with a previous study by Bayrakli et al., in which FISH analysis of clival chordomas showed deletion or amplification of 3p12-p14 in 2 of 6 primary and 2 of 10 recurrent tumors [15]. Furthermore, it is interesting to note that the chromosome 3 loss is observed in a recurrent clival chordoma (CHD20) but not in the primary tumor sample (CHD19). An association between chromosome 3 aberration on cytogenetic analysis of skull base chordomas and both high tumor recurrence rate and decreased survival time has been reported [11].

The ~1.5-Mb *FHIT* gene is found at 3p14.2 and is contained within a common fragile site (FRA3B), rendering it susceptible to deletion breakpoints and rearrangements induced by environmental carcinogens or replicative stress [46–49]. The FRA3B fragile site is not associated with triplet nucleotide repeats but contains adenine-thymine (AT)-dinucleotide-rich sequences that produce high DNA helix flexibility and generate secondary structures that can impede DNA replication [49]. Other mechanisms for instability at the FRA3B site include paucity of replication initiation events [50], late replication [51], inefficient activation of origins of replication [52], and formation of RNA transcript/DNA hybrid complexes [53]. Deletions involving *FHIT* have been reported in small cell and non–small cell lung cancer [39], pancreatic adenocarcinoma [54], head and neck squamous cell carcinoma

[55], esophageal adenocarcinoma [56], and renal cell carcinoma [57]. Furthermore, loss of FHIT expression and aberrant transcripts are found in glioblastoma multiforme and breast cancer [58–60]. Spontaneous tumors arise in both homozygous and heterozygous *FHIT* knockout mice [61]. *FHIT* encodes a 147 amino acid cytoplasmic protein that functions enzymatically as a diadenosine 5′,5′″-P1,P3-triphosphate hydrolase, catalyzing the cleavage of P(1)-P(3)-bis(5′-adenosyl) triphosphate to yield AMP and ADP [62]. However, the tumor suppressor function of FHIT does not appear to require hydrolase activity because mutant FHIT with amino acid substitution at the catalytic active site inhibits gastric and lung cancer cell line–derived tumor growth *in vivo* [63].

Multiple antitumor functions for FHIT have been described including transcriptional regulation of the cell cycle [64,65], modulation of DNA damage checkpoint response [66,67], and enhancement of mitochondrial calcium uptake triggered by apoptosis-inducing factors [68]. We observed a high rate of reduced or absent FHIT protein expression in sacral (98%) and skull base chordomas (67%), but only 21% of classic clival chordomas demonstrated a chromosomal loss or gain encompassing the *FHIT* locus. This suggests that epigenetic mechanisms in addition to genomic instability are involved in the determination of FHIT expression in chordoma. Both of these mechanisms may also be important in chordoma pathogenesis. Support for epigenetic regulation of the *FHIT* locus in cancer cells is the observation that even in the absence of DNA or RNA alterations, FHIT protein expression was found to be absent or reduced in some cancer cell lines [69]. In lung cancer, breast cancer, and clear cell renal carcinoma, loss of *FHIT* gene expression correlates with DNA methylation within a 5′ CpG island [70,71]. Furthermore, in esophageal squamous cell carcinoma cell lines showing transcriptional repression of *FHIT*, the 5′ CpG island of *FHIT* is

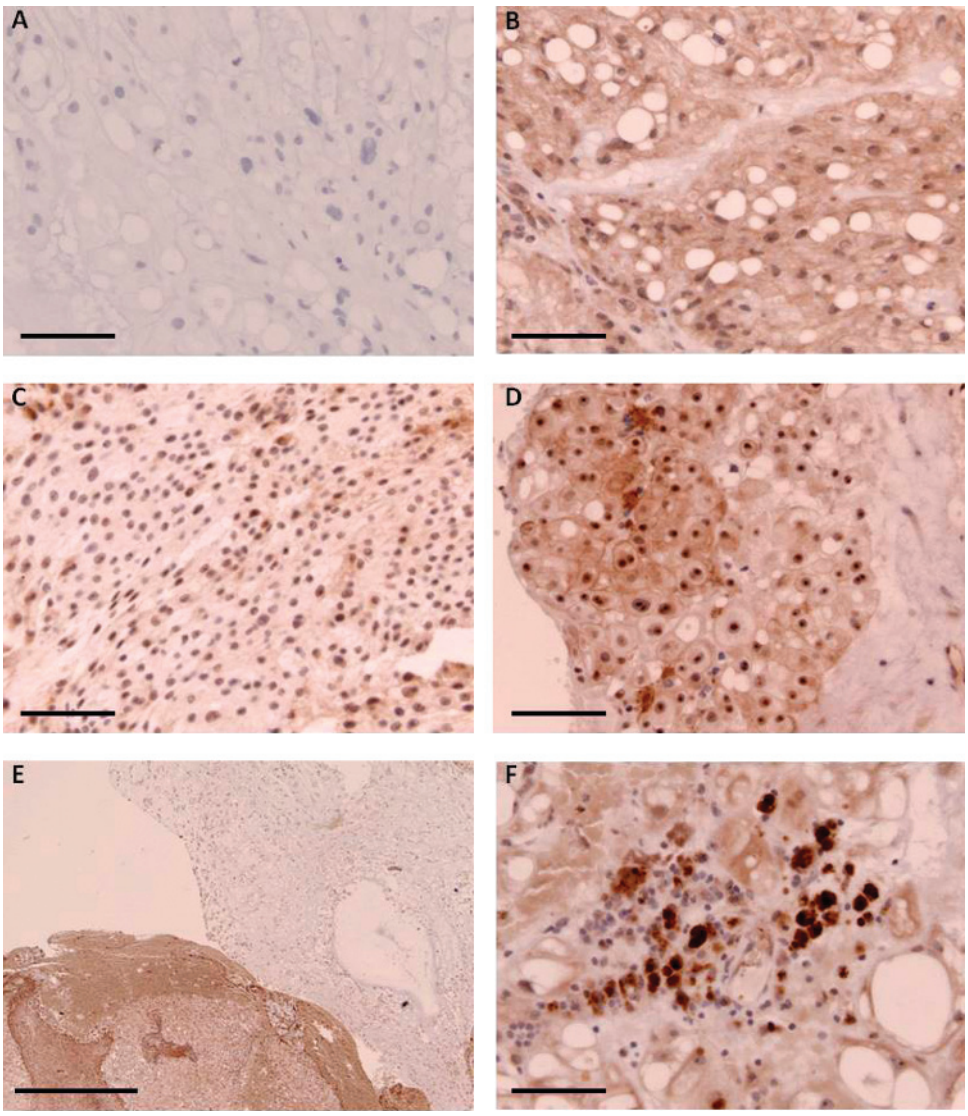

Figure 6. Immunostaining for FHIT protein in four different classic clival chordomas. (A) Secondary antibody–only control; scale bar, 50 μm. (B) Moderate staining in a region of physaliferous cells, 22-year-old female; scale bar, 50 μm. (C) Minimal cytoplasmic staining and moderate nucleolar staining in a tumor from a 39-year-old female; scale bar, 50 μm. (D) Intense staining of nucleoli and variable cytoplasmic staining in a tumor from a 78-year-old male; scale bar, 50 μm. (E) Regions of moderate cytoplasmic staining juxtaposed with regions of no cytoplasmic staining in a recurrent tumor from a 44-year-old male; scale bar, 0.5 mm. (F) Intense cytoplasmic and nuclear staining in tumor-associated macrophages; scale bar, 50 μm.

Table 2. Comparison of Tumor Location, Patient Age, and Recurrent Copy Number Alterations in Copy Number Studies of Chordomas.

Study	Diaz et al. (this study)	Le et al. [33]	Hallor et al. [12]	Scheil et al. [19]
Total number of tumors	22	20	26	16
Location				
Clivus	21	2	0	5
Mobile spine	1	7	2	1
Sacrum	0	11	24*	10
Primary samples	19	17	18	7
Median age (years)	38	61.5	60	61
Platform	Affymetrix 500K	Agilent 250K	BAC array CGH	CGH
Broad significance copy number changes† (frequency)				
Gains			1q21.1-q25.2; 1q31.3-q43	
			5p15.33; 5q31.1-q31.2; 5q35.1-q35.3	5q (0.38)
			6q25.3-q27	
	7 (0.68)	7p36.3-p22.3 (0.25)	7	7q (0.69)
		8q24.3 (0.35)	8q24.21-q24.22	
		11q12.2-q13.4 (0.30)		
			12p13.33-p12.1; 12q13.11-q13.13	12q (0.38)
			15q11.2	
			16q21-q22.2	
		17q11.1-q25.3 (0.25)		
	19p (0.55); 19q (0.55)	19p13.3-q13.43 (0.30)	19p13.3-p13.2; 19q12-q13.43	
			20q11.21-q13.12; 20q13.33	20 (0.50)
Losses			1p36.33-p11.1	1p (0.44)
			2q34-q37.3	
	3 (0.45)	3p29-p26.3 (0.75)	3	3p (0.5)
		4p16.3-q35.2 (0.40)	4	
		6q21-q22.33 (0.25)	6p21.1	
			7q11.22-q11.23	
			8p12-p11.1	
		9p24.3-q34.3 (0.25)	9p24.3-q31.3; 9q33.3-q34.3	
	10p (0.61); 10q (0.57)	10p15.3-q26.3 (0.65)	10	
		11p15.5-p11.12 (0.30)	11p15.5-p15.3; 11p14.3-p11.2; 11q12.2-q13.2; 11q14.3-q25	
			12p11.21-p11.1; 12q24.31	
	13q (0.61)	13q11-q34 (0.60)	13	
	14q (0.65)	14q11.1-q32.33 (0.65)	14	
			15q11.2; 15q15.1-q21.1	
			16p13.3; 16p12.3-q24.3	
		17p13.3-p11.1 (0.35)	17p13.3-p11.1; 17q25.1-q21.3	
		18p11.32-q23 (0.40)	18	
			19p13.3-p11	
			19q13.11-q13.43	
			20p11.21-q11.21	
	22q (0.71)	22q11.1-q13.33 (0.45)		
			21q22.2-q22.3	
			Xp22.33	
			Yp11.2; Yq11.22-q11.23	

*Includes 4 coccyx chordomas and 20 sacral chordomas.
†All four studies differ in the reporting of significant broad copy number alterations. We use *z*-scores of >2 or <0.5 and *q*-values < 0.05 regardless of frequency. Long et al. list copy changes occurring in >25% of cases. Hallor et al. report copy changes occurring in greater than or equal to five cases with individual frequencies not provided. Scheil et al. reports the most frequent gains and losses.

methylated [72]. Treatment of these cells with 5-aza-2′-deoxycytidine resulted in demethylation and *FHIT* mRNA transcription [72]. Bisulfite sequencing of the 5′ CpG island at the *FHIT* locus in skull base and sacral chordoma surgical specimens and concurrent evaluation of *FHIT* mRNA and protein expression will further define the extent to which epigenetic changes contribute to chordoma pathogenesis. Because aberrant *FHIT* transcripts have been previously reported in other tumor types and we observe protein mislocalization to nucleoli rather than cytoplasm in clival chordomas, analysis of *FHIT* mRNA transcripts may provide further details as to FHIT protein dysfunction in chordoma. It has not escaped our notice that reactivation of *FHIT* gene transcription by the use of DNA methyltransferase and/or histone deacetylase inhibitors could open new therapeutic options for patients with chordomas showing loss of FHIT expression without chromosomal deletion. Furthermore, the FHIT deficiency in chordomas may explain the biologic resistance of chordomas to ionizing radiation as it has been shown that *FHIT* gene inactivation increases cell survival after DNA damage by activation of DNA checkpoints regulated by the ataxia telangiectasia-related protein kinase (ATR)/checkpoint kinase 1 (CHK1) pathway [73]. In chordomas with deletion of the *FHIT* gene, reintroduction of *FHIT* gene expression by viral or nonviral methods could potentially render the tumor radiosensitive. Interestingly, adenoviral vector expression of FHIT in tumor cells has been shown to induce apoptosis and impair the growth of non–small cell lung cancer [74], breast cancer [75], esophageal cancer [76], and pancreatic cancer [77] in animal models.

Whole-genome SNP analysis of skull base chordomas demonstrates that these tumors share similar pathogenetic mechanisms that involve loss of cell cycle checkpoint regulation and activation of signaling pathways involved in embryonic stem cell signaling. Despite these similarities, it appears that skull base chordomas have less frequent recurrent focal deletions and amplifications than sacral chordomas. Furthermore, loss of FHIT expression is more common in sacral than skull base chordomas and appears to be a feature of recurrent skull base chordomas. As such, loss of the tumor suppressor effects of FHIT could be an early or

predisposing event in sacral chordomas and a feature associated with therapy resistance in chordomas of the skull base. We describe for the first time a specific gene (*FHIT*) in the chromosome 3 short arm, for which loss of gene expression is a frequent feature of both sacral and skull base chordomas. The absence or reduced expression of FHIT in sacral and skull base chordomas suggests a possible new therapeutic target for treatment of this ultimately debilitating and lethal tumor and provides new insight into chordoma pathogenesis and radioresistance.

Acknowledgments

Tumor database support was provided by Jim Loukides, Arthur and Sonia Labatt Brain Tumor Research Centre, The Hospital for Sick Children. Tissue microarray material was made available from the Royal National Orthopaedic Hospital Musculoskeletal Research Programme and Biobank. Assistance received from Josh Sommer, Chordama Foundation. This work was supported by the Wiley Fund at the Hospital for Sick Children, and the Laurie Berman fund for brain tumor research.

References

[1] McMaster ML, Goldstein AM, Bromley CM, Ishibe N, and Parry DM (2001). Chordoma: incidence and survival patterns in the United States, 1973–1995. *Cancer Causes Control* **12**, 1–11.

[2] Dorfman HD and Czerniak B (1995). Bone cancers. *Cancer* **75**, 203–210.

[3] Eriksson B, Gunterberg B, and Kindblom LG (1981). Chordoma. A clinicopathologic and prognostic study of a Swedish national series. *Acta Orthop Scand* **52**, 49–58.

[4] Higinbotham NL, Phillips RF, Farr HW, and Hustu HO (1967). Chordoma. Thirty-five-year study at Memorial Hospital. *Cancer* **20**, 1841–1850.

[5] Catton C, O'Sullivan B, Bell R, Laperriere N, Cummings B, Fornasier V, and Wunder J (1996). Chordoma: long-term follow-up after radical photon irradiation. *Radiother Oncol* **41**, 67–72.

[6] Chambers PW and Schwinn CP (1979). Chordoma. A clinicopathologic study of metastasis. *Am J Clin Pathol* **72**, 765–776.

[7] Baratti D, Gronchi A, Pennacchioli E, Lozza L, Colecchia M, Fiore M, and Santinami M (2003). Chordoma: natural history and results in 28 patients treated at a single institution. *Ann Surg Oncol* **10**, 291–296.

[8] Diaz RJ and Cusimano MD (2011). The biological basis for modern treatment of chordoma. *J Neurooncol* **104**, 411–422.

[9] Ares C, Hug EB, Lomax AJ, Bolsi A, Timmermann B, Rutz HP, Schuller JC, Pedroni E, and Goitein G (2009). Effectiveness and safety of spot scanning proton radiation therapy for chordomas and chondrosarcomas of the skull base: first long-term report. *Int J Radiat Oncol Biol Phys* **75**, 1111–1118.

[10] Noel G, Feuvret L, Calugaru V, Dhermain F, Mammar H, Haie-Meder C, Ponvert D, Hasboun D, Ferrand R, Nauraye C, et al. (2005). Chordomas of the base of the skull and upper cervical spine. One hundred patients irradiated by a 3D conformal technique combining photon and proton beams. *Acta Oncol* **44**, 700–708.

[11] Almefty KK, Pravdenkova S, Sawyer J, and Al-Mefty O (2009). Impact of cytogenetic abnormalities on the management of skull base chordomas. *J Neurosurg* **110**, 715–724.

[12] Hallor KH, Staaf J, Jonsson G, Heidenblad M, Vult von Steyern F, Bauer HC, Ijszenga M, Hogendoorn PC, Mandahl N, Szuhai K, et al. (2008). Frequent deletion of the *CDKN2A* locus in chordoma: analysis of chromosomal imbalances using array comparative genomic hybridisation. *Br J Cancer* **98**, 434–442.

[13] Longoni M, Orzan F, Stroppi M, Boari N, Mortini P, and Riva P (2008). Evaluation of 1p36 markers and clinical outcome in a skull base chordoma study. *Neuro Oncol* **10**, 52–60.

[14] Sawyer JR, Husain M, and Al-Mefty O (2001). Identification of isochromosome 1q as a recurring chromosome aberration in skull base chordomas: a new marker for aggressive tumors? *Neurosurg Focus* **10**, E6.

[15] Bayrakli F, Guney I, Kilic T, Ozek M, and Pamir MN (2007). New candidate chromosomal regions for chordoma development. *Surg Neurol* **68**, 425–430; discussion 430.

[16] Eisenberg MB, Woloschak M, Sen C, and Wolfe D (1997). Loss of heterozygosity in the retinoblastoma tumor suppressor gene in skull base chordomas and chondrosarcomas. *Surg Neurol* **47**, 156–160; discussion 160-151.

[17] Gil Z, Fliss DM, Voskoboinik N, Leider-Trejo L, Spektor S, Yaron Y, and Orr-Urtreger A (2004). Cytogenetic analysis of three variants of clival chordoma. *Cancer Genet Cytogenet* **154**, 124–130.

[18] Kuzniacka A, Mertens F, Strombeck B, Wiegant J, and Mandahl N (2004). Combined binary ratio labeling fluorescence *in situ* hybridization analysis of chordoma. *Cancer Genet Cytogenet* **151**, 178–181.

[19] Scheil S, Bruderlein S, Liehr T, Starke H, Herms J, Schulte M, and Moller P (2001). Genome-wide analysis of sixteen chordomas by comparative genomic hybridization and cytogenetics of the first human chordoma cell line, U-CH1. *Genes Chromosomes Cancer* **32**, 203–211.

[20] Long F, Sun W, Ji X, Li XH, Liu XQ, Jiang WT, and Tao J (2011). Clinical application of multiplex ligation-dependent probe amplification for the detection exonic copy number alterations in the Dystrophin gene. *Zhonghua Yi Xue Yi Chuan Xue Za Zhi* **28**, 699–704.

[21] Heffelfinger MJ, Dahlin DC, MacCarty CS, and Beabout JW (1973). Chordomas and cartilaginous tumors at the skull base. *Cancer* **32**, 410–420.

[22] Rosenberg AE, Brown GA, Bhan AK, and Lee JM (1994). Chondroid chordoma—a variant of chordoma. A morphologic and immunohistochemical study. *Am J Clin Pathol* **101**, 36–41.

[23] Northcott PA, Nakahara Y, Wu X, Feuk L, Ellison DW, Croul S, Mack S, Kongkham PN, Peacock J, Dubuc A, et al. (2009). Multiple recurrent genetic events converge on control of histone lysine methylation in medulloblastoma. *Nat Genet* **41**, 465–472.

[24] Li C and Wong WH (2001). Model-based analysis of oligonucleotide arrays: expression index computation and outlier detection. *Proc Natl Acad Sci USA* **98**, 31–36.

[25] Lin M, Wei LJ, Sellers WR, Lieberfarb M, Wong WH, and Li C (2004). dChipSNP: significance curve and clustering of SNP-array-based loss-of-heterozygosity data. *Bioinformatics* **20**, 1233–1240.

[26] Yamamoto G, Nannya Y, Kato M, Sanada M, Levine RL, Kawamata N, Hangaishi A, Kurokawa M, Chiba S, Gilliland DG, et al. (2007). Highly sensitive method for genomewide detection of allelic composition in nonpaired, primary tumor specimens by use of Affymetrix single-nucleotide-polymorphism genotyping microarrays. *Am J Hum Genet* **81**, 114–126.

[27] Marshall CR, Noor A, Vincent JB, Lionel AC, Feuk L, Skaug J, Shago M, Moessner R, Pinto D, Ren Y, et al. (2008). Structural variation of chromosomes in autism spectrum disorder. *Am J Hum Genet* **82**, 477–488.

[28] Venkatraman ES and Olshen AB (2007). A faster circular binary segmentation algorithm for the analysis of array CGH data. *Bioinformatics* **23**, 657–663.

[29] Robinson JT, Thorvaldsdottir H, Winckler W, Guttman M, Lander ES, Getz G, and Mesirov JP (2011). Integrative genomics viewer. *Nat Biotechnol* **29**, 24–26.

[30] Pamir MN and Ozduman K (2008). Tumor-biology and current treatment of skull-base chordomas. *Adv Tech Stand Neurosurg* **33**, 35–129.

[31] Hruban RH, Traganos F, Reuter VE, and Huvos AG (1990). Chordomas with malignant spindle cell components. A DNA flow cytometric and immunohistochemical study with histogenetic implications. *Am J Pathol* **137**, 435–447.

[32] Schoedel KE, Martinez AJ, Mahoney TM, Contis L, and Becich MJ (1995). Chordomas: pathological features; ploidy and silver nucleolar organizing region analysis. A study of 36 cases. *Acta Neuropathol* **89**, 139–143.

[33] Le LP, Nielsen GP, Rosenberg AE, Thomas D, Batten JM, Deshpande V, Schwab J, Duan Z, Xavier RJ, Hornicek FJ, et al. (2011). Recurrent chromosomal copy number alterations in sporadic chordomas. *PLoS One* **6**, e18846.

[34] Presneau N, Shalaby A, Ye H, Pillay N, Halai D, Idowu B, Tirabosco R, Whitwell D, Jacques TS, Kindblom LG, et al. (2011). Role of the transcription factor *T* (brachyury) in the pathogenesis of sporadic chordoma: a genetic and functional-based study. *J Pathol* **223**, 327–335.

[35] Hsu W, Mohyeldin A, Shah SR, ap Rhys CM, Johnson LF, Sedora-Roman NI, Kosztowski TA, Awad OA, McCarthy EF, Loeb DM, et al. (2011). Generation of chordoma cell line JHC7 and the identification of Brachyury as a novel molecular target. *J Neurosurg* **115**, 760–769.

[36] Yang XR, Ng D, Alcorta DA, Liebsch NJ, Sheridan E, Li S, Goldstein AM, Parry DM, and Kelley MJ (2009). *T* (brachyury) gene duplication confers major susceptibility to familial chordoma. *Nat Genet* **41**, 1176–1178.

[37] Aydemir E, Bayrak OF, Sahin F, Atalay B, Kose GT, Ozen M, Sevli S, Dalan AB, Yalvac ME, Dogruluk T, et al. (2012). Characterization of cancer stem-like cells in chordoma. *J Neurosurg* **116**, 810–820.

[38] Sozzi G, Tornielli S, Tagliabue E, Sard L, Pezzella F, Pastorino U, Minoletti F, Pilotti S, Ratcliffe C, Veronese ML, et al. (1997). Absence of Fhit protein in primary lung tumors and cell lines with *FHIT* gene abnormalities. *Cancer Res* **57**, 5207–5212.

[39] Fong KM, Biesterveld EJ, Virmani A, Wistuba I, Sekido Y, Bader SA, Ahmadian M, Ong ST, Rassool FV, Zimmerman PV, et al. (1997). FHIT

and FRA3B 3p14.2 allele loss are common in lung cancer and preneoplastic bronchial lesions and are associated with cancer-related FHIT cDNA splicing aberrations. *Cancer Res* **57**, 2256–2267.

[40] Naylor SL, Johnson BE, Minna JD, and Sakaguchi AY (1987). Loss of heterozygosity of chromosome 3p markers in small-cell lung cancer. *Nature* **329**, 451–454.

[41] Hibi K, Takahashi T, Yamakawa K, Ueda R, Sekido Y, Ariyoshi Y, Suyama M, Takagi H, and Nakamura Y (1992). Three distinct regions involved in 3p deletion in human lung cancer. *Oncogene* **7**, 445–449.

[42] Yamakawa K, Morita R, Takahashi E, Hori T, Ishikawa J, and Nakamura Y (1991). A detailed deletion mapping of the short arm of chromosome 3 in sporadic renal cell carcinoma. *Cancer Res* **51**, 4707–4711.

[43] Maestro R, Gasparotto D, Vukosavljevic T, Barzan L, Sulfaro S, and Boiocchi M (1993). Three discrete regions of deletion at 3p in head and neck cancers. *Cancer Res* **53**, 5775–5779.

[44] Kohno T, Takayama H, Hamaguchi M, Takano H, Yamaguchi N, Tsuda H, Hirohashi S, Vissing H, Shimizu M, Oshimura M, et al. (1993). Deletion mapping of chromosome 3p in human uterine cervical cancer. *Oncogene* **8**, 1825–1832.

[45] Sato T, Akiyama F, Sakamoto G, Kasumi F, and Nakamura Y (1991). Accumulation of genetic alterations and progression of primary breast cancer. *Cancer Res* **51**, 5794–5799.

[46] Ong ST, Fong KM, Bader SA, Minna JD, Le Beau MM, McKeithan TW, and Rassool FV (1997). Precise localization of the *FHIT* gene to the common fragile site at 3p14.2 (FRA3B) and characterization of homozygous deletions within FRA3B that affect *FHIT* transcription in tumor cell lines. *Genes Chromosomes Cancer* **20**, 16–23.

[47] Huebner K, Hadaczek P, Siprashvili Z, Druck T, and Croce CM (1997). The *FHIT* gene, a multiple tumor suppressor gene encompassing the carcinogen sensitive chromosome fragile site, *FRA3B. Biochim Biophys Acta* **1332**, M65–M70.

[48] Zawacka-Pankau J and Ferens B (2009). Enlightened protein: Fhit tumor suppressor protein structure and function and its role in the toxicity of protoporphyrin IX-mediated photodynamic reaction. *Toxicol Appl Pharmacol* **241**, 246–252.

[49] Ozeri-Galai E, Bester AC, and Kerem B (2012). The complex basis underlying common fragile site instability in cancer. *Trends Genet* **28**, 295–302.

[50] Letessier A, Millot GA, Koundrioukoff S, Lachages AM, Vogt N, Hansen RS, Malfoy B, Brison O, and Debatisse M (2011). Cell-type-specific replication initiation programs set fragility of the *FRA3B* fragile site. *Nature* **470**, 120–123.

[51] Wang L, Darling J, Zhang JS, Huang H, Liu W, and Smith DI (1999). Allele-specific late replication and fragility of the most active common fragile site, FRA3B. *Hum Mol Genet* **8**, 431–437.

[52] Palakodeti A, Lucas I, Jiang Y, Young DJ, Fernald AA, Karrison T, and Le Beau MM (2010). Impaired replication dynamics at the FRA3B common fragile site. *Hum Mol Genet* **19**, 99–110.

[53] Helmrich A, Ballarino M, and Tora L (2011). Collisions between replication and transcription complexes cause common fragile site instability at the longest human genes. *Mol Cell* **44**, 966–977.

[54] Birnbaum DJ, Adelaide J, Mamessier E, Finetti P, Lagarde A, Monges G, Viret F, Goncalves A, Turrini O, Delpero JR, et al. (2011). Genome profiling of pancreatic adenocarcinoma. *Genes Chromosomes Cancer* **50**, 456–465.

[55] Virgilio L, Shuster M, Gollin SM, Veronese ML, Ohta M, Huebner K, and Croce CM (1996). FHIT gene alterations in head and neck squamous cell carcinomas. *Proc Natl Acad Sci USA* **93**, 9770–9775.

[56] Michael D, Beer DG, Wilke CW, Miller DE, and Glover TW (1997). Frequent deletions of *FHIT* and FRA3B in Barrett's metaplasia and esophageal adenocarcinomas. *Oncogene* **15**, 1653–1659.

[57] Sukosd F, Kuroda N, Beothe T, Kaur AP, and Kovacs G (2003). Deletion of chromosome 3p14.2-p25 involving the VHL and FHIT genes in conventional renal cell carcinoma. *Cancer Res* **63**, 455–457.

[58] Cecener G, Tunca B, Egeli U, Bekar A, Guler G, Tolunay S, and Aksoy K (2010). *FHIT* gene sequence variants and reduced Fhit protein expression in glioblastoma multiforme. *Cell Mol Neurobiol* **30**, 301–307.

[59] Gatalica Z, Lele SM, Rampy BA, and Norris BA (2000). The expression of Fhit protein is related inversely to disease progression in patients with breast carcinoma. *Cancer* **88**, 1378–1383.

[60] Hayashi S, Tanimoto K, Hajiro-Nakanishi K, Tsuchiya E, Kurosumi M, Higashi Y, Imai K, Suga K, and Nakachi K (1997). Abnormal FHIT transcripts in human breast carcinomas: a clinicopathological and epidemiological analysis of 61 Japanese cases. *Cancer Res* **57**, 1981–1985.

[61] Zanesi N, Fidanza V, Fong LY, Mancini R, Druck T, Valtieri M, Rudiger T, McCue PA, Croce CM, and Huebner K (2001). The tumor spectrum in *FHIT*-deficient mice. *Proc Natl Acad Sci USA* **98**, 10250–10255.

[62] Barnes LD, Garrison PN, Siprashvili Z, Guranowski A, Robinson AK, Ingram SW, Croce CM, Ohta M, and Huebner K (1996). Fhit, a putative tumor suppressor in humans, is a dinucleoside 5′,5′″-P1,P3-triphosphate hydrolase. *Biochemistry* **35**, 11529–11535.

[63] Siprashvili Z, Sozzi G, Barnes LD, McCue P, Robinson AK, Eryomin V, Sard L, Tagliabue E, Greco A, Fusetti L, et al. (1997). Replacement of Fhit in cancer cells suppresses tumorigenicity. *Proc Natl Acad Sci USA* **94**, 13771–13776.

[64] Ji L, Fang B, Yen N, Fong K, Minna JD, and Roth JA (1999). Induction of apoptosis and inhibition of tumorigenicity and tumor growth by adenovirus vector-mediated fragile histidine triad (*FHIT*) gene overexpression. *Cancer Res* **59**, 3333–3339.

[65] Nishizaki M, Sasaki J, Fang B, Atkinson EN, Minna JD, Roth JA, and Ji L (2004). Synergistic tumor suppression by coexpression of FHIT and p53 coincides with FHIT-mediated MDM2 inactivation and p53 stabilization in human non-small cell lung cancer cells. *Cancer Res* **64**, 5745–5752.

[66] Ishii H, Wang Y, and Huebner K (2007). A Fhit-ing role in the DNA damage checkpoint response. *Cell Cycle* **6**, 1044–1048.

[67] Ishii H, Mimori K, Inoue H, Inageta T, Ishikawa K, Semba S, Druck T, Trapasso F, Tani K, Vecchione A, et al. (2006). Fhit modulates the DNA damage checkpoint response. *Cancer Res* **66**, 11287–11292.

[68] Rimessi A, Marchi S, Fotino C, Romagnoli A, Huebner K, Croce CM, Pinton P, and Rizzuto R (2009). Intramitochondrial calcium regulation by the FHIT gene product sensitizes to apoptosis. *Proc Natl Acad Sci USA* **106**, 12753–12758.

[69] Druck T, Hadaczek P, Fu TB, Ohta M, Siprashvili Z, Baffa R, Negrini M, Kastury K, Veronese ML, Rosen D, et al. (1997). Structure and expression of the human *FHIT* gene in normal and tumor cells. *Cancer Res* **57**, 504–512.

[70] Zochbauer-Muller S, Fong KM, Maitra A, Lam S, Geradts J, Ashfaq R, Virmani AK, Milchgrub S, Gazdar AF, and Minna JD (2001). 5′ CpG island methylation of the *FHIT* gene is correlated with loss of gene expression in lung and breast cancer. *Cancer Res* **61**, 3581–3585.

[71] Kvasha S, Gordiyuk V, Kondratov A, Ugryn D, Zgonnyk YM, Rynditch AV, and Vozianov AF (2008). Hypermethylation of the 5′ CpG island of the *FHIT* gene in clear cell renal carcinomas. *Cancer Lett* **265**, 250–257.

[72] Tanaka H, Shimada Y, Harada H, Shinoda M, Hatooka S, Imamura M, and Ishizaki K (1998). Methylation of the 5′ CpG island of the *FHIT* gene is closely associated with transcriptional inactivation in esophageal squamous cell carcinomas. *Cancer Res* **58**, 3429–3434.

[73] Hu B, Han SY, Wang X, Ottey M, Potoczek MB, Dicker A, Huebner K, and Wang Y (2005). Involvement of the *Fhit* gene in the ionizing radiation-activated ATR/CHK1 pathway. *J Cell Physiol* **202**, 518–523.

[74] Zandi R, Xu K, Poulsen HS, Roth JA, and Ji L (2011). The effect of adenovirus-mediated gene expression of FHIT in small cell lung cancer cells. *Cancer Invest* **29**, 683–691.

[75] Sevignani C, Calin GA, Cesari R, Sarti M, Ishii H, Yendamuri S, Vecchione A, Trapasso F, and Croce CM (2003). Restoration of *fragile histidine triad* (*FHIT*) expression induces apoptosis and suppresses tumorigenicity in breast cancer cell lines. *Cancer Res* **63**, 1183–1187.

[76] Ishii H, Dumon KR, Vecchione A, Trapasso F, Mimori K, Alder H, Mori M, Sozzi G, Baffa R, Huebner K, et al. (2001). Effect of adenoviral transduction of the *fragile histidine triad* gene into esophageal cancer cells. *Cancer Res* **61**, 1578–1584.

[77] Dumon KR, Ishii H, Vecchione A, Trapasso F, Baldassarre G, Chakrani F, Druck T, Rosato EF, Williams NN, Baffa R, et al. (2001). Fragile histidine triad expression delays tumor development and induces apoptosis in human pancreatic cancer. *Cancer Res* **61**, 4827–4836.

Table W1. Broad Significance Copy Number Chromosomal Loss or Gain Analysis for 22 Skull Base Chordomas.

Arm	No. of Genes	Amplification Frequency	Amplification *z*-Score	Amplification *q*-Value	Deletion Frequency	Deletion *z*-Score	Deletion *q*-Value
1p	1423	0	−1.99	0.977	0.39	1.98	0.0899
1q	1274	0.18	−0.459	0.977	0.3	0.83	0.529
2p	590	0.29	0.557	0.805	0.12	−1.14	0.994
2q	1017	0.25	0.244	0.977	0.17	−0.612	0.994
3p	661	0.08	−1.33	0.977	0.45	2.46	0.0304
3q	732	0.08	−1.32	0.977	0.45	2.47	0.0304
4p	291	0.07	−1.57	0.977	0.36	1.37	0.257
4q	667	0.07	−1.43	0.977	0.41	1.95	0.0899
5p	169	0.35	1.14	0.499	0.19	−0.503	0.994
5q	1009	0.35	1.31	0.412	0.19	−0.379	0.994
6p	768	0.3	0.831	0.648	0	−2.19	0.994
6q	550	0.3	0.785	0.648	0	−2.22	0.994
7p	390	0.68	4.9	9.57E − 06	0.12	−0.748	0.994
7q	815	0.68	5.03	9.57E − 06	0.12	−0.709	0.994
8p	370	0.13	−1.21	0.977	0	−2.5	0.994
8q	554	0.13	−1.18	0.977	0	−2.48	0.994
9p	275	0.08	−1.27	0.977	0.5	2.86	0.0137
9q	731	0	−1.9	0.977	0.48	2.8	0.0143
10p	248	0	−1.69	0.977	0.61	4.14	0.000169
10q	817	0	−1.73	0.977	0.57	3.81	0.000537
11p	578	0.2	−0.364	0.977	0.16	−0.788	0.994
11q	1048	0.14	−0.917	0.977	0.1	−1.35	0.994
12p	374	0.14	−1.02	0.977	0.1	−1.45	0.994
12q	943	0.14	−0.933	0.977	0.1	−1.37	0.994
13q	400	0	−1.67	0.977	0.61	4.18	0.000169
14q	874	0	−1.54	0.977	0.65	4.82	2.79E − 05
15q	776	0.16	−0.757	0.977	0.2	−0.33	0.994
16p	585	0.2	−0.363	0.977	0.16	−0.787	0.994
16q	456	0.2	−0.384	0.977	0.16	−0.806	0.994
17p	420	0.43	2.06	0.111	0.14	−0.829	0.994
17q	1086	0.41	2.05	0.111	0.07	−1.38	0.994
18p	93	0.13	−0.987	0.977	0.38	1.48	0.226
18q	265	0.12	−1.07	0.977	0.33	1.01	0.439
19p	721	0.55	3.48	0.00243	0.09	−1.11	0.994
19q	1055	0.55	3.57	0.00228	0.09	−1.07	0.994
20p	249	0.33	0.927	0.627	0.29	0.523	0.733
20q	528	0.37	1.37	0.412	0.25	0.139	0.994
21q	324	0.14	−1.03	0.977	0.1	−1.46	0.994
22q	598	0.55	2.44	0.0575	0.71	4.59	4.25E − 05

Table W2. Focal Deletions and Amplifications in 22 Skull Base Chordomas.

Chromosome	Start	End	Chordoma	Copy Number
1	64010000	64258800	1	2.9785
1	73415100	73597100	1	2.7531
3	1.14E + 08	1.14E + 08	13	3.1337
6	6956840	7041070	6	3.2562
6	1.64E + 08	1.71E + 08	17	2.9556
7	17740800	18224800	8	3.1441
7	21259200	22677900	8	2.848
7	23176700	25324300	8	2.8286
7	26599600	27037100	8	2.7276
7	28169700	28332900	8	2.5539
7	1.05E + 08	1.05E + 08	21	3.6597
8	180568	2290330	3	2.3167
8	2291450	2555870	3	3.0804
10	44557600	44649400	16	2.913
11	18905800	18916600	15	3.6039
11	57188600	57488200	3	3.3231
11	88751000	88984700	18	3.2482
13	64426400	64876100	26	3.018
14	19273000	19492400	2	3.2352
14	19273000	19490000	13	3.3815
14	19273000	19492400	22	3.5283
15	18427100	20329200	6	2.8686
15	19821400	20059900	10	3.1342
16	83196000	83226300	2	3.118
17	6888	595982	23	2.4384
17	31427100	31501500	6	2.9558
17	41006800	41022700	3	3.8239
17	41521600	41647900	3	3.258
18	41802200	42497500	8	2.949
18	54560000	54957300	9	2.7628
19	9911180	12049300	26	3.5655
20	704982	757930	2	3.2953
20	23030400	23093300	3	3.1663
20	29310000	34285700	3	3.2411
20	46286500	46420700	3	2.4006
22	21048600	21487500	1	2.6534
22	26496400	26571300	1	3.4285
22	27558000	27839300	1	2.6784
22	31421600	31600500	1	2.7299
22	38030700	38499900	1	2.7776
22	40758200	41196600	1	2.9287
23	6505280	6662160	6	2.8086
23	7548890	8051920	6	2.4649
1	1.93E + 08	1.96E + 08	11	1.1955
2	1.1E + 08	1.1E + 08	3	0.3366
8	4117730	4203330	13	0.9329
9	10977800	11895600	2	1.222
9	11903200	12061200	17	0.9162
9	21796600	22032000	3	0.3449
9	21805200	22232100	8	1.0207
9	1.19E + 08	1.19E + 08	14	1.2975
10	47030100	47129100	9	0.7324
13	82995900	83045900	14	0.8358
15	18427100	20329200	11	1.3031
15	18427100	20089400	8	1.3899
20	23118700	28143700	3	1.4837
20	45623800	46285300	3	1.5193
22	26574200	27515100	1	1.6995
23	18654	2704240	2	1.1324
23	18654	2700830	10	1.1456
23	18654	2713630	6	1.1662
23	18654	2700830	19	1.19365
23	18654	2700830	22	1.2042
23	18654	2700830	12	1.2055
23	18654	2700830	20	1.2591
23	18654	2713390	14	1.27
23	18654	2700830	8	1.2776
23	18654	2700830	13	1.38107

Deletions marked in blue and amplifications in red.

Figure W1. Analysis of recurrent focal deletion at 9p showing involvement of *CDKN2A*, *CDKN2B*, and *MTAP* genes.